

Unveiling Optimal Diffusion for Infection Control in Brownian Particle Systems

Kaito Takahashi,¹ Makiko Sasada,^{2,*} and Takuma Akimoto^{1,†}

¹*Department of Physics and Astronomy, Tokyo University of Science, Noda, Chiba 278-8510, Japan*

²*Graduate School of Mathematical Sciences, University of Tokyo,*

3-8-1, Komaba, Meguro-ku, Tokyo, 153-8914, Japan

(Dated: February 11, 2025)

Understanding the spread of infectious diseases requires integrating movement and interaction dynamics into epidemiological models. In this study, we investigate the role of particle diffusivity and physical constraints in shaping infection dynamics within a system of Brownian particles. Through numerical simulations and theoretical analyses, we uncover a nontrivial relationship between diffusivity and infection speed: an optimal diffusion coefficient exists that minimizes the infection spreading speed. This counterintuitive result arises from a balance between particle mixing and interaction frequency. The optimal diffusivity is observed in both interacting and non-interacting systems when the infection radius exceeds the mean lattice spacing and the initial configuration is out of equilibrium. Our findings provide a theoretical framework for understanding and controlling the spread of infections in confined and diffusive environments, with potential implications for designing movement-based strategies for infection control.

I. Introduction

Mathematical models for understanding and predicting the spread of infectious diseases play a fundamental role in epidemiology [1]. One of the most classical and widely-used models is the Susceptible-Infected-Recovered (SIR) model, proposed by Kermack and McKendrick in 1927 [2]. This model divides the population into three compartments—susceptible, infected, and recovered—and describes the dynamics of disease spread based on interaction rates among these groups. The SIR model, along with its variants (SIS, SEIR, etc.), has been applied to study various infectious diseases, including influenza and COVID-19 [3–7]. However, these compartmental models often overlook spatial interactions and individual mobility patterns, which are critical factors in realistic simulations of infectious disease dynamics [8, 9].

To address these limitations, spatial models have been developed to incorporate local interactions and individual movement patterns [10–12]. For instance, the spatial SIR model assumes that infections occur only within a defined spatial range, creating heterogeneous infection patterns that depend on spatial constraints. Recently, particle-based models have attracted attention for their ability to simulate infection dynamics in mobile populations, where individual movement influences transmission [13–17]. These models are based on physical principles of particle dynamics and allow for a detailed analysis of how contact patterns and movement affect disease spread.

Recent developments in active matter physics provide a framework for understanding collective motion in non-equilibrium systems. Active matter systems, composed of self-propelling particles, exhibit emergent behaviors such as flocking and clustering due to local interactions

[18]. Notably, the Vicsek model demonstrates how alignment interactions lead to coherent group behavior [19], and this framework has been adapted to simulate infection dynamics [20–22].

Certain active matter systems also incorporate Lévy walk-like dynamics [23], characterized by intermittent long-range displacements. Lévy walks, with their heavy-tailed displacement distributions, are widely used to model large-scale movement patterns in ecological and epidemiological contexts [24], such as animal search strategies and pathogen spread [25, 26]. While Lévy walks and active matter share similarities, especially in systems with intermittent or correlated motion, our study focuses on Brownian motion [27]. Unlike Lévy walks, Brownian motion is isotropic and short-ranged, making it better suited for investigating infection dynamics in confined environments. By examining the role of diffusivity and exclusion volume effects in Brownian motion, our work bridges the gap between particle-level dynamics and macroscopic infection patterns, complementing studies of active matter and Lévy walks.

In this study, we model infectious disease dynamics using N Brownian particles, where each particle can be in either an infected or susceptible state, mimicking spin dynamics on moving lattice points. Specifically, we examine how the diffusion coefficient of the Brownian particle and infection radius affect the progression of infection. Additionally, we analyze how interactions between particles influence infection dynamics, taking into account the presence or absence of excluded volume effects. We aim to clarify how the speed of infection progression and patterns of infection spread change through numerical simulations and theoretical analysis.

II. Model

We investigate infection propagation in a one-dimensional system containing N Brownian particles un-

* sasada@ms.u-tokyo.ac.jp

† takuma@rs.tus.ac.jp

der periodic boundary conditions with a system length L . Initially, the particles are evenly spaced with an inter-particle distance of L/N . In later sections, we explore how alternative initial conditions affect the infection dynamics. The motion of each particle follows standard Brownian dynamics, governed by the following stochastic differential equation [28, 29]:

$$\dot{x}_i(t) = \xi(t) \quad (1)$$

where $x_i(t)$ is a position of i -th Brownian particle, $\xi(t)$ represents Gaussian white noise with zero mean, characterized by a diffusion coefficient D that governs the particle's mobility. The noise $\xi(t)$ satisfies the fluctuation-dissipation relation [30]:

$$\langle \xi(t) \rangle = 0, \quad \langle \xi(t)\xi(t') \rangle = 2D\delta(t-t') \quad (2)$$

where $\langle \cdot \rangle$ denotes the ensemble average, and $\delta(t-t')$ is the Dirac delta function.

A. Exclusion Volume Effect

We examine two scenarios: interacting and non-interacting Brownian particles. In the interacting case, particles experience an exclusion volume effect, which prevents them from passing through each other. This phenomenon, known as single-file diffusion in one-dimensional systems, ensures that particle order remains fixed during motion [31, 32]. As a result, neighboring particles are unable to overtake each other, and their spatial order is maintained throughout the dynamics, preventing overlap [33]. Consequently, single-file diffusion leads to sub-diffusive behavior, where the mean square displacement (MSD) grows as $t^{1/2}$ instead of the linear growth in normal diffusion [34–38]. This constraint plays a significant role in modulating infection propagation, as infection can only spread sequentially among neighboring particles.

B. Infection Propagation Model and Infection Probability

In this study, we adopt the Susceptible-Infected (SI) model to describe the process of infection propagation [39]. Each particle (agent) possesses one of two states: “susceptible” or “infected.” A susceptible particle may become infected if it resides within the infection radius r of an infected particle. When particle interactions are present, and a single-file spatial constraint is imposed, the exclusion volume effect governs the infection propagation. In this case, infection can only spread to adjacent particles; infection cannot leap over other particles, even if the susceptible particle lies within the infection radius r . On the other hand, in non-interacting systems, the exclusion volume effect is not present, and infection can leap over adjacent particles. In this scenario, even if a

susceptible particle is separated by multiple neighbors, it can still become infected if it lies within the infection radius r . This distinction results in different infection propagation patterns and speeds between single-file systems and non-interacting systems.

As an initial condition for infection, a single infected particle is placed at the center of the agent distribution, while all other particles are susceptible. The state of infection for the j -th particle at time t is denoted by $s_j(t)$, where $s_j(t) = 1$ indicates the particle is infected, and $s_j(t) = 0$ indicates it is susceptible [39, 40]. Additionally, the indicator function $\sigma_{ij}(t)$ is used to determine whether particle i is within the infection radius of particle j . For non-interacting systems, $\sigma_{ij}(t)$ is defined as

$$\sigma_{ij}(t) = \begin{cases} 1 & \text{if } |x_i(t) - x_j(t)| < r, \\ 0 & \text{otherwise.} \end{cases} \quad (3)$$

In the interacting systems, $\sigma_{ij}(t)$ is modified to account for the exclusion volume effect:

$$\sigma_{ij}(t) = \begin{cases} 1 & \text{if } |x_i(t) - x_j(t)| < r \text{ and } |i - j| = 1, \\ 0 & \text{otherwise.} \end{cases} \quad (4)$$

This modification implies that in interacting systems, infections cannot leap over neighboring particles. As a result, the exclusion volume effect restricts the spatial propagation of infection.

The infection propagates as a Poisson process [41, 42], where the probability of a susceptible particle i becoming infected during the interval $[t, t + \Delta t]$ is given by

$$P_{infected} = 1 - \exp\left(-\beta \sum_{j=1}^N \sigma_{ij}(t) s_j(t) \Delta t\right), \quad (5)$$

assuming that the value of $\sigma_{ij}(t)$ remains constant within $[t, t + \Delta t]$. Here, β represents the infection rate. This expression depends on the number of infected neighboring particles and the susceptible particles within the infection radius. To simplify this expression, in the limit of $\Delta t \rightarrow 0$, where $\beta \sum_{j=1}^N \sigma_{ij}(t) s_j(t) \Delta t \ll 1$, the infection probability can be approximated as

$$P_{infected} \approx \beta \sum_{j=1}^N \sigma_{ij}(t) s_j(t) \Delta t. \quad (6)$$

This linear approximation highlights that the infection probability depends on the number of infected neighboring particles, the infection rate, and the time step Δt . While the motion of particles are continuous, the simulations discretize time into sufficiently small intervals. This ensures the accuracy of the infection dynamics. For interacting systems, the exclusion volume effect restricts $\sigma_{ij}(t)$ to nonzero values only for adjacent particles ($|i - j| = 1$), preventing the infection from leaping over intermediate particles. In contrast, non-interacting systems allow the infection to spread freely, with $\sigma_{ij}(t)$ determined solely by the spatial distance $|x_i(t) - x_j(t)|$.

C. Simulation Process

The simulation proceeds in two phases, repeated iteratively to simulate infection propagation and particle movement:

1. **Infection phase:** The infection process is applied to all particles simultaneously. If a susceptible particle lies within the infection radius of an infected particle, it becomes infected with probability $P_{infected} = \beta \sum_{j=1}^N \sigma_{ij}(t) s_j(t) \Delta t$. This probability is calculated independently for each particle, and the procedure is repeated for all particles in the system during each time step.
2. **Particle movement phase:** Each particle then undergoes a displacement based on the Brownian dynamics described in Eq. (1). In systems with exclusion volume effects, particles may exchange positions if necessary to prevent overlap.

By alternating between these two phases, we simulate the interaction between diffusion and infection, allowing us to explore how the diffusion coefficient and particle interactions influence the infection propagation speed.

III. Results

We investigate how the diffusivity of particles and the infection radius affect the infection speed in systems of N Brownian particles with and without interactions, where the initial particle configuration is a lattice arrange. To evaluate the infection speed, we define the relaxation time τ as the time required for half of the particles to become infected. Using this relaxation time, we can estimate the infection speed throughout the system, thus capturing the temporal dynamics of how the infection spreads. We examine how the relaxation time τ is determined by the diffusion coefficient D and the infection radius r for a fixed infection rate of $\beta = 0.05$, where the density is also fixed as $\rho = N/L = 0.1$, with $N = 10^2$ and $L = 10^3$. The infection radius defines the range within which an infected particle can infect others, significantly impacting the spread of infection.

A. The Role of Infection Radius in Diffusion-Controlled Systems

Our simulations of both interacting and non-interacting Brownian particle systems reveal a clear and consistent relationship between the infection radius r and the infection relaxation time τ . Figures 1(a) and (b) show the heatmap of the relaxation time in (r, D) space, demonstrating its dependence on both r and the diffusion coefficient D .

For both interacting and non-interacting systems, the relaxation time τ decreases monotonically with increas-

ing r across all values of D , with this trend being particularly pronounced in the low-diffusivity regime. This behavior arises because a larger infection radius allows each infected particle to interact with and infect more susceptible neighbors within its vicinity, thereby accelerating the overall spread of infection.

B. Optimal Diffusivity for Infection Control

Our simulations reveal the existence of an optimal diffusion coefficient that maximizes the infection relaxation time, effectively minimizing the infection spreading speed in both interacting and non-interacting systems. This counterintuitive behavior emerges from a delicate balance between particle mixing and interaction frequency.

When the infection radius r is fixed, the relaxation time τ exhibits two distinct regimes, indicating that the infection dynamics strongly depend on the diffusion coefficient D and exhibits two different patterns.

In the first regime, where the infection radius r is smaller than a threshold r^* , the relaxation time τ decreases monotonically with increasing D . Numerical simulation reveal that the threshold r^* is determined by the interparticle spacing of the initial lattice configuration, L/N . This threshold radius is nearly identical across both interacting and non-interacting systems, approximately equal to $r^* \approx L/N = 10$ under the simulation conditions. This monotonically decreasing trend implies that higher diffusivity enhances the rate of infection spread by increasing the likelihood of contact between infected and susceptible particles. In this low-radius regime, limited contact opportunities dominate the dynamics, making diffusion essential for accelerating infection [see Figs. 1(c) and (d)].

In contrast, when the infection radius r exceeds the threshold r^* , a more complex behavior emerges. At zero diffusion ($D = 0$), the relaxation time is relatively short as infection progresses via static proximity. However, in the low-diffusive regime, τ increases, suggesting that limited mobility temporarily hinders the spread of infection. As the diffusion coefficient increases further, the relaxation time decreases again and eventually converges. This behavior indicates the existence of an intermediate, optimal diffusion coefficient that maximizes the relaxation time. The non-trivial peak in τ reflects the intricate interplay between particle mixing and infection interactions [see Figs. 1(c) and (d)]. Moreover, increasing the infection radius r shifts the peak of the relaxation time to a high diffusivity, indicating that the diffusion coefficient D at which the relaxation time is the longest becomes larger. This phenomenon further highlights the influence of the infection radius on particle dynamics and infection spreading.

These findings highlight the complexity of infection dynamics and demonstrate that controlling diffusivity can significantly impact the spread of infections, with potential applications in designing effective containment

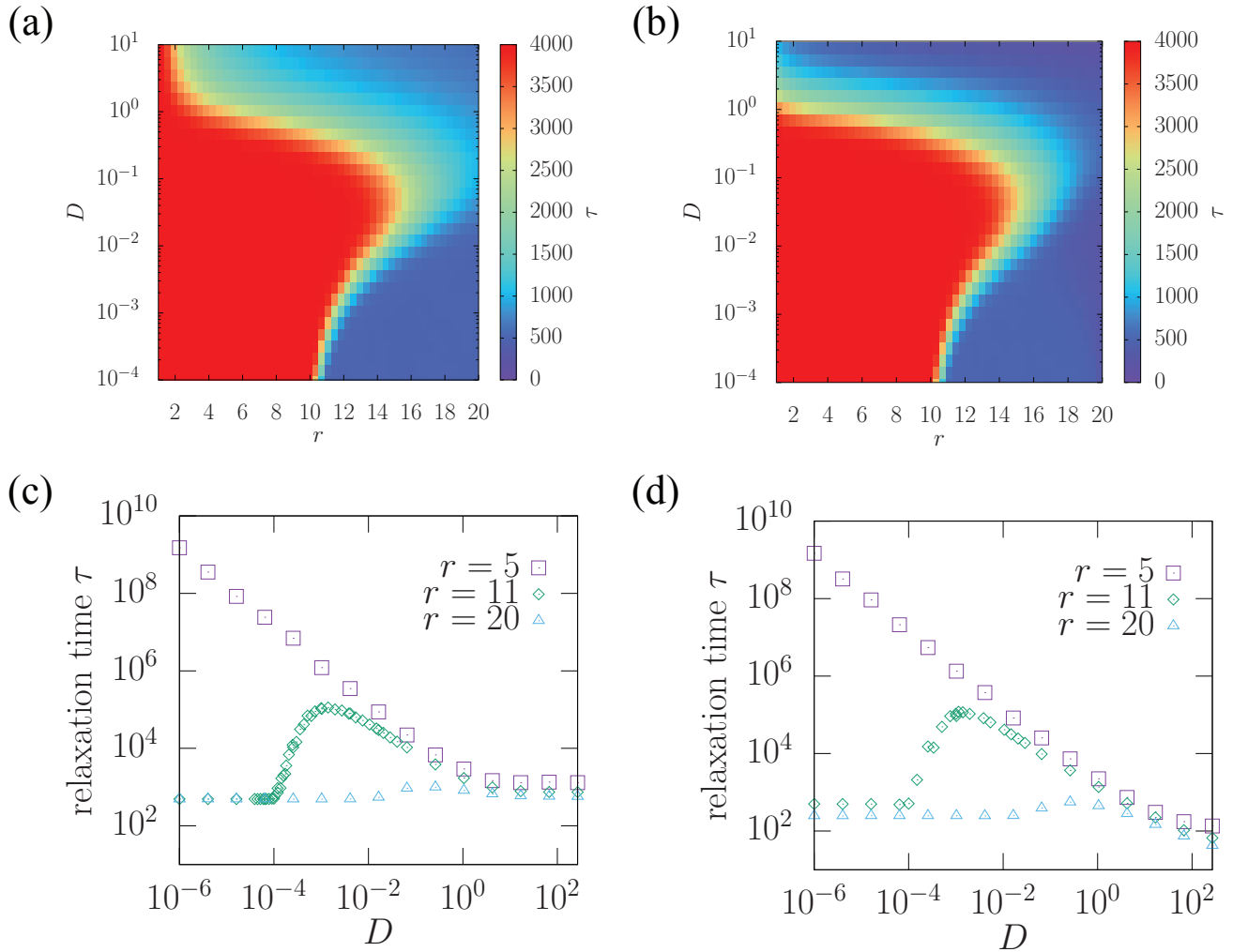


FIG. 1: Infection relaxation time τ with infection rate $\beta = 0.05$, $L = 10^3$, and $N = 10^2$, where the initial particle configuration is a lattice arrange. (a) Heatmap of infection relaxation time in interacting system, (b) Heatmap of infection relaxation time in non-interacting system, (c) Infection relaxation time τ as a function of the diffusion coefficient D in interacting system for different values of r , and (d) Infection relaxation time τ as a function of the diffusion coefficient D in non-interacting system for different values of r . The symbols are the results of numerical simulations.

strategies.

C. Impact of Exclusion Volume on Infection Dynamics

Volume-exclusion interactions suppress particle diffusivity and influence the infection relaxation time in high-diffusivity regime. As shown in Figs. 1(c) and (d), the infection relaxation time τ in non-interacting systems exhibits behavior similar to that observed in interacting systems. The threshold r^* , which marks the transition in infection dynamics, remains consistent between the two cases.

For Low-diffusivity regime, no significant difference in the relaxation time τ is observed between interacting and non-interacting systems. This is because, in the low-diffusivity regime, when adjacent susceptible particles come into contact with infected particles, infection occurs within the infection radius before the susceptible particles pass the infected particles, resulting in the minimal influence of inter-particle interactions.

At higher diffusion coefficients, the relaxation time τ asymptotically converges to a lower value in non-interacting systems compared to interacting systems. Theoretical results for the high-diffusivity limit ($D = \infty$) confirm this trend (see Appendix B). This reflects the enhanced ability of fast diffusion to facilitate rapid mix-

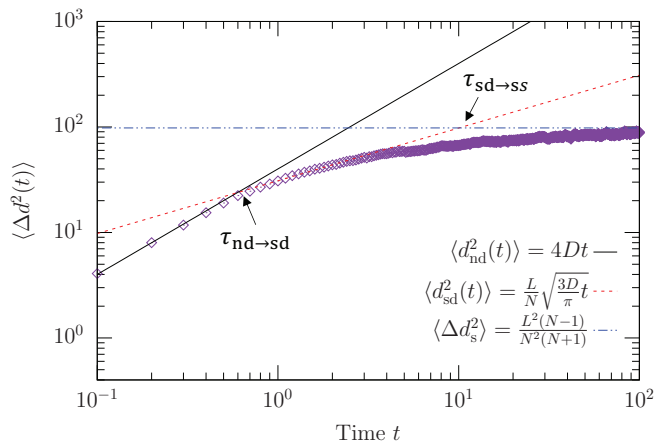


FIG. 2: Mean square change in the distance of neighboring particles in a single-file system as a function of time. Symbols are the results of numerical simulations. The simulation parameters are $N = 100$, $L = 1000$, $D = 10$ with integration time step of $dt = 0.01$, where the initial configuration of the particles is a lattice arrangement and the ensemble average is performed under these conditions. Three lines represent $\langle d_{nd}^2(t) \rangle = 4Dt$, $\langle d_{sd}^2(t) \rangle = \frac{L}{N} \sqrt{\frac{3D}{\pi} t}$, and $\langle \Delta d_s^2 \rangle = \frac{L^2(N-1)}{N^2(N+1)}$ is the theoretical value in the steady state.

ing and infection spread when particles are not constrained by interactions [see Figs. 1(c) and (d)]. Additionally, a leapover effect emerges in the infection dynamics, where susceptible particles bypass intermediate infected particles, further enhancing the infection speed in non-interacting systems.

These findings underscore the significant role of exclusion volume effects in moderating infection dynamics. Physical constraints in interacting systems suppress the spread of infection by limiting it to sequential interactions. In contrast, non-interacting systems achieve faster mixing and propagation under high-diffusivity conditions, promoting rapid infection spread by enhancing particle mobility and mixing.

IV. Discussion

We investigate how optimal diffusivity emerges in both interacting and non-interacting systems by analyzing three characteristic timescales of diffusion dynamics and comparing them with the infection relaxation time. To characterize the diffusive characteristic timescales, we examine the mean square change in the distance (MSCD) of neighboring particles, defined as $\langle \Delta d^2(t) \rangle$, where $\Delta d^2(t) = (d(t) - d(0))^2$ and $d(t) = x_{i+1}(t) - x_i(t)$. As shown in Fig. 2, the MSCD in a single-file system transitions over time from normal diffusion to subdiffu-

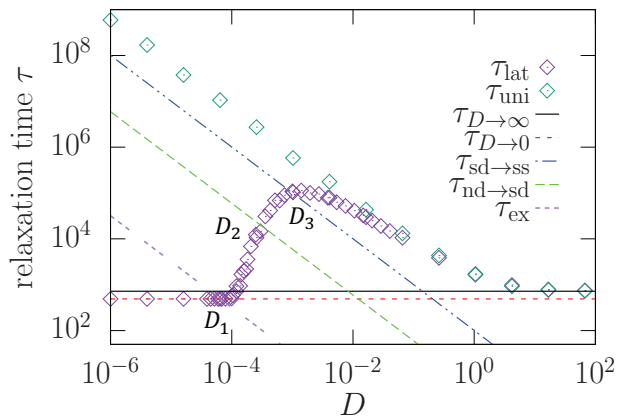


FIG. 3: Initial configuration dependence of infection relaxation time in the interacting system, where the parameters are the same as in Fig. 1. Relaxation times τ_{lat} and τ_{uni} are calculated from the initial configurations with lattice configuration and the uniform distribution. Solid lines represent the theoretical predictions of the relaxation times $\tau_{D \rightarrow 0}$ and $\tau_{D \rightarrow \infty}$ for low and high diffusivity limit, respectively. Three lines represent three characteristic time scales τ_{ex} , $\tau_{nd \rightarrow sd}$ and $\tau_{sd \rightarrow ss}$ as a function of D , i.e., where Eqs. (9), (7) and (8).

sion and eventually to a steady state.

We quantify two timescales to characterize the transitions in particle dynamics: the transition time from normal diffusion to subdiffusion, $\tau_{nd \rightarrow sd}$, and the crossover time from subdiffusion to the steady state, $\tau_{sd \rightarrow ss}$. These timescales are determined by identifying the crossover points in the MSCD. These crossover points correspond to the intersections of theoretical MSCD curves for normal diffusion ($\langle d_{nd}^2(t) \rangle = 4Dt$), subdiffusion ($\langle d_{sd}^2(t) \rangle = \frac{L}{N} \sqrt{\frac{3D}{\pi} t}$), and the steady state (see Appendix C). The characteristic timescales are given by the following expressions:

$$\tau_{nd \rightarrow sd} = \left(\frac{L}{N} \right)^2 \frac{3}{16\pi D}, \quad (7)$$

and

$$\tau_{sd \rightarrow ss} = \left\{ \frac{L(N-1)}{N(N+1)} \right\}^2 \frac{\pi}{3D}. \quad (8)$$

Both timescales are inversely proportional to the diffusion coefficient, D^{-1} , indicating a clear physical relationship between the diffusion coefficient and the relaxation dynamics.

Additionally, we introduce a characteristic escape time, related to the mean fastest first passage time (MFFPT). This time describes the time required for distance between two Brownian particles, among $N/2$ independent Brownian particles initially separated by $x_{i+1}(0) -$

$x_i(0) = L/N$, to reach the threshold $|x_{i+1}(t) - x_i(t)| = r$. The MFFPT is derived in [43–46] as

$$\tau_{\text{ex}} = \frac{(r - L/N)^2}{8D \ln(N/2)}. \quad (9)$$

Although there are two targets located at $x_{i+1}(t) - x_i(t) = r$ and $x_{i+1}(t) - x_i(t) = -r$, the fastest particle’s passage time is primarily dictated by the closest boundary at $x_{i+1}(t) - x_i(t) = r$, as the influence of the more distant target is negligible. This escape time is also inversely proportional to the diffusion coefficient (D^{-1}), emphasizing the role of diffusivity in determining how quickly two particles can separate to a critical distance.

The infection relaxation time exhibits a strong dependence on the initial particle configuration, especially in the low-diffusivity regime. Figure 3 shows how the infection relaxation time varies with the diffusion coefficient for different initial conditions in the interacting systems. When the initial configuration is a steady state (uniform distribution), the infection relaxation time decreases significantly as D increases. In this scenario, stronger diffusion enhances particle-particle interactions, thereby accelerating the spread of infection. In contrast, when the initial configuration is a lattice arrangement, the infection relaxation time shows a more complex dependence on D . Specifically, in the low-diffusion regime, the infection relaxation time is much smaller than the particle diffusion relaxation time $\tau_{\text{sd} \rightarrow \text{ss}}$, indicating that infection dynamics are dominated by the initial configuration. As shown in Fig. 3, three transition diffusivities— D_1 , D_2 , and D_3 —characterize the behavior of the infection relaxation time.

1. **First transition point (D_1):** At D_1 , the infection relaxation time τ_{lat} begins to increase with D . Below D_1 , the infection relaxation time remains nearly constant, showing little dependence on D . This point corresponds to the condition where the infection relaxation time matches the escape time, τ_{ex} , for $N/2$ particles starting at L/N . When the infection relaxation time exceeds τ_{ex} , a “link” in the infection chain breaks, causing a rise in the infection relaxation time. The diffusion coefficient D_1 can be derived as the intersection between τ_{ex} and $\tau_{D \rightarrow 0}$ (see Appendix A):

$$D_1 = \frac{(r - L/N)^2 \beta}{2 \ln(N/2)(N - 2)}. \quad (10)$$

This equation shows that D_1 depends quadratically on the infection radius r ; as r increases, D_1 also increases quadratically due to the longer escape time for susceptible particles. As shown in Fig. 3, the theoretical prediction aligns well with the simulation results.

2. **Second transition point (D_2):** Beyond D_1 , as the diffusion coefficient increases, more particles escape the initial infection region, temporarily slowing the infection rate and increasing the infection

relaxation time. This trend begins to moderate at D_2 . For $D > D_2$, particle interactions become significant, creating a confinement effect characteristic of single-file systems. As a result, the infection relaxation time becomes smaller than $\tau_{\text{nd} \rightarrow \text{sd}}$, the time scale associated with the transition from normal diffusion to subdiffusion. In this regime, the confinement imposed by particle interactions reduces the escape rate, leading to a stabilization of the infection spreading speed. As shown in Fig. 3, this stabilization begins when the infection relaxation time matches $\tau_{\text{nd} \rightarrow \text{sd}}$.

3. **Third transition point (D_3):** Beyond D_3 , as the diffusion coefficient increases, the infection relaxation time begins to decrease with D . In this regime, the particle configuration relaxation time $\tau_{\text{sd} \rightarrow \text{ss}}$ becomes comparable to the infection relaxation time. As a result, for $D > D_3$, the infection relaxation time is no longer influenced by the initial configuration, leading to a decrease in relaxation time and the emergence of a peak. As shown in Fig. 3, the theoretical prediction aligns well with the simulation results. Notably, since the MSCD is identical in both interacting and non-interacting systems, the particle configuration relaxation time $\tau_{\text{sd} \rightarrow \text{ss}}$ remains unchanged. While the mechanisms of infection spreading differ between interacting and non-interacting systems, the third transition point is consistent across both systems.

These results highlight the intricate interplay between diffusion dynamics, particle interactions, and initial configurations in determining infection relaxation times. By identifying these key transition points, we provide a robust framework for understanding optimal diffusivity in controlling infection speed.

V. Conclusion

We have performed numerical simulations to unveil how the infection radius and particle diffusivity significantly affect the infection spreading. Specifically, when the infection radius is smaller than L/N , the infection relaxation time decreases monotonically with respect to the diffusion coefficient. This behavior occurs because the frequency of particle contacts increases due to high diffusivity, allowing the infection to spread more rapidly. On the other hand, when the infection radius exceeds L/N , a nontrivial peak in the infection relaxation time was observed, indicating the existence of an optimal diffusion coefficient. This peak suggests that if diffusion is either too slow or too fast, the infection spread speed becomes high, and there exists a specific diffusivity that is most effective in suppressing the infection. This insight can serve as a useful guideline for designing infection control strategies by appropriately limiting movement and contact.

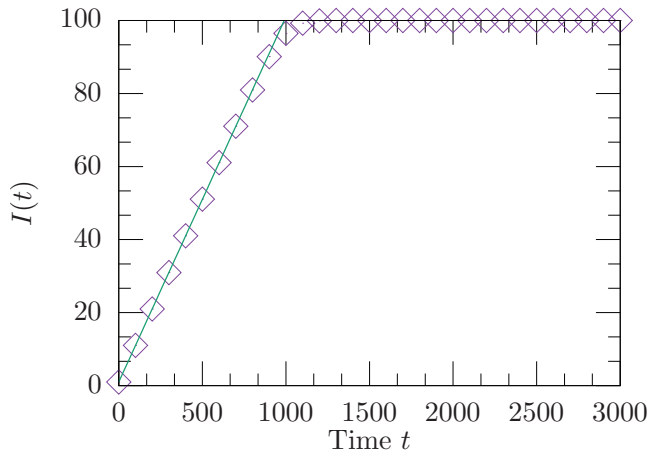


FIG. 4: Time evolution of the number of infected particles $I(t)$ in the static limit ($D = 0$), with $N = 100$, $L = 1000$, $\beta = 0.05$ and the initial state arranged on a lattice. The graph compares simulation results with the theoretical prediction given by Eq. (A4).

Additionally, we investigated the difference in infection dynamics with and without the exclusion volume effect, quantitatively evaluating the impact of particle interactions on the spread of infection. In the presence of the exclusion volume effect, physical contact between particles is restricted, leading to a tendency for slower infection spread. In contrast, when the exclusion volume effect is absent, the infection spreads more rapidly. This result highlights the significant impact of physical constraints on infection dynamics in real-world scenarios and provides implications for practical infection control measures, such as social distancing and movement restrictions.

The findings of this study offer a new perspective on understanding the mechanisms of infection spread, especially by providing a theoretical basis for explaining how physical constraints and diffusivity affect infection dynamics.

Appendix

A. Infection dynamics in the low-diffusive limit ($D = 0$) in interacting systems

In the low-diffusive limit, infected particles remain fixed and do not move. Once an infected individual appears in the system, there is always a constant number of susceptible particles within the infection radius throughout the entire system. Specifically, since susceptible particles remain within a range of two particle lengths from the infected, the number of susceptible particles within the infection radius is always 2.

To describe the time evolution of the probability $p_k(t)$ that there are k infected particles at time t , the following

master equation [47, 48] can be established:

$$\begin{cases} \frac{dP_1(t)}{dt} = -2\beta P_1(t) \\ \frac{dP_k(t)}{dt} = 2\beta P_{k-1}(t) - 2\beta P_k(t) \quad (2 \leq k \leq N-1) \\ \frac{dP_N(t)}{dt} = 2\beta P_{N-1}(t). \end{cases} \quad (\text{A1})$$

The equations represent the dynamic process of the number of infected particles increasing or decreasing, allowing us to analyze the changes in the number of infected over time. Solving the master equation yields

$$\begin{cases} P_k(t) = \frac{(2\beta t)^{k-1}}{(k-1)!} e^{-2\beta t}, \quad (1 \leq k \leq N-1), \\ P_N(t) = 1 - \sum_{k=1}^{N-1} P_k(t). \end{cases} \quad (\text{A2})$$

The mean number of infected people at time t is given by

$$\langle I(t) \rangle = \sum_{k=1}^N k P_k(t). \quad (\text{A3})$$

For $N \gg 1$, $\langle I(t) \rangle$ can be approximated as

$$\langle I(t) \rangle \approx 2\beta t + 1. \quad (\text{A4})$$

This approximated result is in a good agreement with numerical simulations (see Fig. 4). From this result, the infection relaxation time $\tau_{D \rightarrow 0}$ is obtained as

$$\tau_{D \rightarrow 0} = \frac{N-2}{4\beta}. \quad (\text{A5})$$

This result is exact, despite the use of an approximation in the expression for $\langle I(t) \rangle$, as the infection dynamics follow a Poisson process.

B. Infection dynamics in the high-diffusive limit ($D = \infty$) in the interacting system

In the high-diffusive limit, particle interactions play a significant role due to the exclusion volume effect. In this regime, particles are arranged in a steady state characterized by a uniform distribution. The PDF $P(d)$ of the distance d between two neighboring particles in a single-file diffusion system can be expressed as

$$P(d) = \frac{N-1}{L} \left(1 - \frac{d}{L}\right)^{N-2}, \quad (\text{B1})$$

where N is the number of particles, and L is the total system length. The shape of this distribution becomes steeper as the number of particles N increases, reflecting the higher particle density. Using this PDF, the probability that the distance x between any two adjacent particles is within the infection radius r can be computed. This probability determines the average number of susceptible

particles $\langle n_s \rangle$ in contact with an infected particle, which is given by

$$\langle n_s \rangle = 2 \int_0^r P(x) dx = 2 \left\{ 1 - \left(1 - \frac{r}{L} \right)^{N-1} \right\}. \quad (\text{B2})$$

For $N \gg 1$, $\langle n_s \rangle$ asymptotically approaches 2, indicating that, on average, there are two susceptible particles within the infection radius at the boundary of the infected cluster.

With this result, the master equation for the number of infected particles $I(t)$ in the high-diffusive limit can be expressed as

$$\frac{dP_k(t)}{dt} = \beta \langle n_s \rangle [P_{k-1}(t) - P_k(t)], \quad (\text{B3})$$

where β is the infection rate and $P_k(t)$ is the probability of having k infected particles at time t . Solving this equation using the same approach as in Appendix A yields the time evolution of the expected number of infected particles as

$$\langle I(t) \rangle = 2\beta \left\{ 1 - \left(1 - \frac{r}{L} \right)^{N-1} \right\} t + 1. \quad (\text{B4})$$

This result is in a good agreement with numerical simulations (see Fig. 5). From this result, the infection relaxation time $\tau_{D \rightarrow \infty}$ is obtained as

$$\tau_{D \rightarrow \infty} = \frac{N - 2}{4\beta \left\{ 1 - \left(1 - \frac{r}{L} \right)^{N-1} \right\}} \quad (\text{B5})$$

This expression provides an analytical representation of the temporal evolution of the number of infected particles in the high-diffusive limit, taking interactions into account. Including interactions between particles is predicted to significantly change the speed and pattern of infection progression.

C. Theory of interparticle distance in single-file systems

1. Mean square change in distance of two neighboring particles in the steady state

In the long-time limit, the mean square change in the distance (MSCD) between two neighboring particles converges to the variance of their distance in the steady state. Using the PDF of interparticle distance $P(d)$, i.e., Eq. (B1), the variance of the distance can be calculated as

$$\langle \Delta d_s^2 \rangle = \int_0^L \left(x - \frac{L}{N} \right)^2 P(x) dx, \quad (\text{C1})$$

where $d - \frac{L}{N}$ represents the deviation of the particle distance d from the mean particle spacing $\frac{L}{N}$. Performing this integration yields

$$\langle \Delta d_s^2 \rangle = \frac{L^2(N-1)}{N^2(N+1)}. \quad (\text{C2})$$

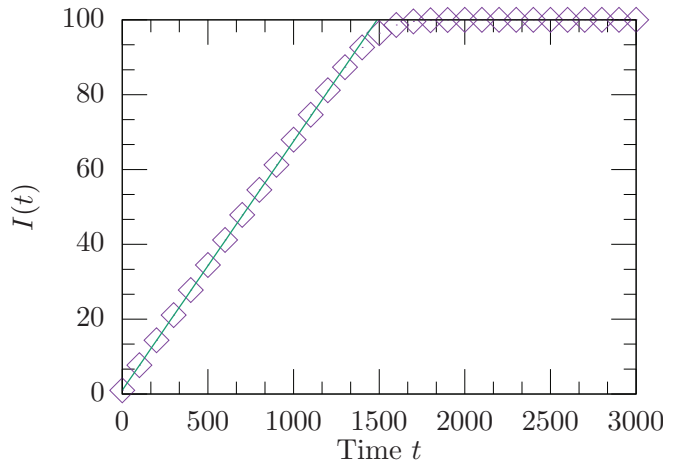


FIG. 5: Time evolution of the number of infected particles $I(t)$ in the interactive case ($D = \infty$), with $N = 100$, $L = 1000$, and the initial state arranged on a lattice. The graph compares simulation results with the theoretical prediction given by Eq. (B4).

This result shows that the MSCD depends on both the number of particles N and the system length L . As N increases, the fluctuations in the distance between neighboring particles decrease, indicating that the system becomes more tightly packed. This theoretical result serves as a reference value for the steady-state behavior, which can be compared with numerical simulation results.

2. Dynamics of two-particle distance in single-file systems and transition points

The dynamics of the distance between two particles in single-file diffusion systems exhibit distinct behaviors depending on the time scale. This subsection examines the theoretical transition points from normal diffusion to subdiffusion and from subdiffusion to the steady state.

The mean square distance between two neighboring particles can be expressed as

$$\langle d^2(t) \rangle = \langle (x_{i+1}(t) - x_i(t))^2 \rangle = 2\langle x_i^2(t) \rangle - 2\langle x_{i+1}(t)x_i(t) \rangle, \quad (\text{C3})$$

where $d(t) = x_{i+1}(t) - x_i(t)$ is the distance between two neighboring particles and $\langle x_{i+1}(t)x_i(t) \rangle$ represents the correlation function between neighboring particles. At the initial stages of diffusion, this correlation is negligible and the diffusion is normal. Therefore, the MSCD in the initial stage of diffusion can be approximated as

$$\langle \Delta d^2(t) \rangle \approx \langle d_{\text{nd}}^2(t) \rangle = 4Dt, \quad (\text{C4})$$

where D is the diffusion coefficient.

As time progresses, particles begin to experience the effects of the single-file constraint, causing their motion to transition from normal diffusion to subdiffusion. This

phenomenon is particularly noticeable in systems initialized with a lattice configuration. In this subdiffusive regime, the MSD of a single particle is known to asymptotically follow subdiffusion [49–51]:

$$\langle (x_i(t) - x_i(0))^2 \rangle \sim \frac{L}{N} \sqrt{\frac{2D}{\pi}} \sqrt{t}, \quad (\text{C5})$$

where L is the system length and N is the number of particles. This subdiffusive behavior reflects the impact of particle interactions in the single-file system. During this stage, the correlation function $\langle x_{i+1}(t)x_i(t) \rangle$ between neighboring particles becomes significant and cannot be neglected in calculating the MSCD. Numerical simulations reveal that the MSCD grows proportionally to \sqrt{t} in this regime. Fitting the MSD using the form of Eq. (C5) shows that the coefficient of the diffusion term is approximately 3. Therefore, the MSCD in the subdiffusive regime is expressed as

$$\langle \Delta d^2(t) \rangle \approx \langle d_{\text{sd}}^2(t) \rangle = \frac{L}{N} \sqrt{\frac{3D}{\pi}} \sqrt{t}. \quad (\text{C6})$$

This subdiffusive behavior is transient, as the MSCD eventually converges to a constant value determined by the steady state of the system.

Using Eqs. (C4) and (C6), the crossover time from nor-

mal diffusion to subdiffusion is given by

$$\tau_{\text{nd} \rightarrow \text{sd}} = \left(\frac{L}{N} \right)^2 \frac{3}{\pi} \frac{1}{16D}. \quad (\text{C7})$$

This equation indicates that the crossover time depends on the system size L , the number of particles N , and the diffusion coefficient D . As N increases, the crossover occurs at shorter time scales, and a larger D further accelerates this transition. These results highlight the shift from independent motion to motion constrained by the single-file structure.

As time progresses further, the system eventually reaches a steady state. The MSCD in the steady state is theoretically given by Eq. (C2). From this, the diffusion relaxation time for the transition from subdiffusion to the steady state is obtained as

$$\tau_{\text{sd} \rightarrow \text{ss}} = \left\{ \frac{L(N-1)}{N(N+1)} \right\}^2 \frac{\pi}{3D}. \quad (\text{C8})$$

This result indicates that the relaxation time depends strongly on the system size L , particle number N , and diffusion coefficient D . Specifically, as N increases, the time required to reach the steady state becomes shorter, while a larger D shortens the relaxation time.

-
- [1] Marc Choisy, Jean-François Guégan, and Pejman Rohani. Mathematical modeling of infectious diseases dynamics. Encyclopedia of infectious diseases: modern methodologies, 379, 2007.
 - [2] William Ogilvy Kermack and Anderson G McKendrick. A contribution to the mathematical theory of epidemics. Proceedings of the royal society of london. Series A, Containing papers of a mathematical and physical character, 115(772):700–721, 1927.
 - [3] R Anderson. Infectious diseases of humans: dynamics and control. Cambridge University Press, 1991.
 - [4] Esteban A Hernandez-Vargas, Esther Wilk, Laetitia Canini, Franklin R Toapanta, Sebastian C Binder, Alexey Uvarovskii, Ted M Ross, Carlos A Guzmán, Alan S Perelson, and Michael Meyer-Hermann. Effects of aging on influenza virus infection dynamics. Journal of virology, 88(8):4123–4131, 2014.
 - [5] Shaobo He, Yuexi Peng, and Kehui Sun. Seir modeling of the covid-19 and its dynamics. Nonlinear dynamics, 101:1667–1680, 2020.
 - [6] Jeff Bartlett, James Deviney, and Eric Pudlowski. Mathematical modeling of the 2014/2015 ebola epidemic in west africa. SIAM Undergraduate Research Online, 9:87–102, 2016.
 - [7] Syafruddin Side and Salmi Md Noorani. A sir model for spread of dengue fever disease (simulation for south sulawesi, indonesia and selangor, malaysia). World Journal of Modelling and Simulation, 9(2):96–105, 2013.
 - [8] Ian Cooper, Argha Mondal, and Chris G Antonopoulos. A sir model assumption for the spread of covid-19 in different communities. Chaos, Solitons & Fractals, 139:110057, 2020.
 - [9] Linda JS Allen. Some discrete-time si, sir, and sis epidemic models. Mathematical biosciences, 124(1):83–105, 1994.
 - [10] Herbert W Hethcote. The mathematics of infectious diseases. SIAM review, 42(4):599–653, 2000.
 - [11] Sebastian Funk, Marcel Salathé, and Vincent AA Jansen. Modelling the influence of human behaviour on the spread of infectious diseases: a review. Journal of the Royal Society Interface, 7(50):1247–1256, 2010.
 - [12] Mikio Shibuya. On infection spreading between independent brownian motions. Kyushu Journal of Mathematics, 64(2):181–197, 2010.
 - [13] Jorge P Rodríguez, Fakhteh Ghanbarnejad, and Víctor M Eguíluz. Particle velocity controls phase transitions in contagion dynamics. Scientific reports, 9(1):6463, 2019.
 - [14] Jorge P Rodríguez, Matteo Paoluzzi, Demian Levis, and Michele Starnini. Epidemic processes on self-propelled particles: Continuum and agent-based modeling. Physical Review Research, 4(4):043160, 2022.
 - [15] Marek Laskowski, Bryan CP Demianyk, Julia Witt, Shamir N Mukhi, Marcia R Friesen, and Robert D McLeod. Agent-based modeling of the spread of influenza-like illness in an emergency department: a simulation study. IEEE Transactions on Information Technology in Biomedicine, 15(6):877–889, 2011.
 - [16] Petrônio CL Silva, Paulo VC Batista, Hélder S Lima, Marcos A Alves, Frederico G Guimarães, and Rodrigo CP Silva. Covid-abs: An agent-based model of

- covid-19 epidemic to simulate health and economic effects of social distancing interventions. Chaos, Solitons & Fractals, 139:110088, 2020.
- [17] Pablo de Castro, Felipe Urbina, Ariel Norambuena, and Francisca Guzmán-Lastra. Sequential epidemic-like spread between agglomerates of self-propelled agents in one dimension. Phys. Rev. E, 108:044104, Oct 2023.
- [18] M. C. Marchetti, J. F. Joanny, S. Ramaswamy, T. B. Liverpool, J. Prost, Madan Rao, and R. Aditi Simha. Hydrodynamics of soft active matter. Rev. Mod. Phys., 85:1143–1189, Jul 2013.
- [19] Tamás Vicsek, András Czirók, Eshel Ben-Jacob, Inon Cohen, and Ofer Shochet. Novel type of phase transition in a system of self-driven particles. Phys. Rev. Lett., 75:1226–1229, Aug 1995.
- [20] Ariel Norambuena, Felipe J Valencia, and Francisca Guzmán-Lastra. Understanding contagion dynamics through microscopic processes in active brownian particles. Scientific Reports, 10(1):20845, 2020.
- [21] PM Centres, DJ Perez-Morelo, R Guzman, L Reinaudi, and MC Gimenez. Diffusion model for the spread of infectious diseases: Sir model with mobile agents. Physica A: Statistical Mechanics and its Applications, 633:129399, 2024.
- [22] Siyang Cai, Yongmei Cai, and Xuerong Mao. A stochastic differential equation sis epidemic model with two correlated brownian motions. Nonlinear Dynamics, 97:2175–2187, 2019.
- [23] V. Zaburdaev, S. Denisov, and J. Klafter. Lévy walks. Rev. Mod. Phys., 87:483–530, Jun 2015.
- [24] Matt J Keeling and Pejman Rohani. Modeling infectious diseases in humans and animals. Princeton university press, 2011.
- [25] Gandhimohan M Viswanathan, Vsevolod Afanasyev, Sergey V Buldyrev, Eugene J Murphy, Peter A Prince, and H Eugene Stanley. Lévy flight search patterns of wandering albatrosses. Nature, 381(6581):413–415, 1996.
- [26] Frederic Bartumeus, M G E da Luz, Gandhimohan M Viswanathan, and Jordi Catalan. Animal search strategies: a quantitative random-walk analysis. Ecology, 86(11):3078–3087, 2005.
- [27] Albert Einstein et al. On the motion of small particles suspended in liquids at rest required by the molecular-kinetic theory of heat. Annalen der physik, 17(549-560):208, 1905.
- [28] George E Uhlenbeck and Leonard S Ornstein. On the theory of the brownian motion. Physical review, 36(5):823, 1930.
- [29] IID Nulton, P Salamon, RK Pathria, et al. Correlation in the langevin theory of brownian motion. Am. J. Phys, 61(10):10, 1993.
- [30] Rep Kubo. The fluctuation-dissipation theorem. Reports on progress in physics, 29(1):255, 1966.
- [31] Markus Kollmann. Single-file diffusion of atomic and colloidal systems: asymptotic laws. Physical review letters, 90(18):180602, 2003.
- [32] Christoph Lutz, Markus Kollmann, and Clemens Bechinger. Single-file diffusion of colloids in one-dimensional channels. Physical review letters, 93(2):026001, 2004.
- [33] Jerome K Percus. Anomalous self-diffusion for one-dimensional hard cores. Physical Review A, 9(1):557, 1974.
- [34] Theodore E Harris. Diffusion with “collisions” between particles. Journal of Applied Probability, 2(2):323–338, 1965.
- [35] Vishwas Gupta, Sriram S Nivarthi, Alon V McCormick, and H Ted Davis. Evidence for single file diffusion of ethane in the molecular sieve alpo4-5. Chemical Physics Letters, 247(4-6):596–600, 1995.
- [36] Kärger Hahn, Jörg Kärger, and Volker Kukla. Single-file diffusion observation. Physical review letters, 76(15):2762, 1996.
- [37] Volker Kukla, Jan Kornatowski, Dirk Demuth, Irina Girnus, Harry Pfeifer, Lovat VC Rees, Stefan Schunk, Klaus K Unger, and Jörg Kärger. Nmr studies of single-file diffusion in unidimensional channel zeolites. Science, 272(5262):702–704, 1996.
- [38] Jörg Kärger. Straightforward derivation of the long-time limit of the mean-square displacement in one-dimensional diffusion. Physical Review A, 45(6):4173, 1992.
- [39] Ágnes Bodó, Gyula Y Katona, and Péter L Simon. Sis epidemic propagation on hypergraphs. Bulletin of mathematical biology, 78:713–735, 2016.
- [40] Ginestra Bianconi. Epidemic spreading and bond percolation on multilayer networks. Journal of Statistical Mechanics: Theory and Experiment, 2017(3):034001, 2017.
- [41] Daryl J Daley and Joseph Mark Gani. Epidemic modelling: an introduction. Number 15. Cambridge University Press, 1999.
- [42] Frank Ball and Peter Neal. A general model for stochastic sir epidemics with two levels of mixing. Mathematical biosciences, 180(1-2):73–102, 2002.
- [43] George H Weiss, Kurt E Shuler, and Katja Lindenberg. Order statistics for first passage times in diffusion processes. Journal of Statistical Physics, 31:255–278, 1983.
- [44] SB Yuste and L Acedo. Diffusion of a set of random walkers in euclidean media. first passage times. Journal of Physics A: Mathematical and General, 33(3):507, 2000.
- [45] Santos B Yuste, L Acedo, and Katja Lindenberg. Order statistics for d-dimensional diffusion processes. Physical Review E, 64(5):052102, 2001.
- [46] Santos B Yuste and Luis Acedo. Order statistics of the trapping problem. Physical Review E, 64(6):061107, 2001.
- [47] Nico Stollenwerk and Keith M Briggs. Master equation solution of a plant disease model. Physics Letters A, 274(1-2):84–91, 2000.
- [48] Daniel Sanchez-Taltavull, Violeta Castelo-Szekely, Daniel Candinas, Edgar Roldan, and Guido Beldi. Modelling strategies to organize healthcare workforce during pandemics: Application to covid-19. Journal of theoretical biology, 523:110718, 2021.
- [49] Ludvig Lizana, Tobias Ambjörnsson, Alessandro Taloni, Eli Barkai, and Michael A Lomholt. Foundation of fractional langevin equation: harmonization of a many-body problem. Physical Review E—Statistical, Nonlinear, and Soft Matter Physics, 81(5):051118, 2010.
- [50] Benjamin Sorkin and David S Dean. Uphill drift in the absence of current in single-file diffusion. Physical Review Letters, 133(10):107101, 2024.
- [51] N Leibovich and E Barkai. Everlasting effect of initial conditions on single-file diffusion. Physical Review E—Statistical, Nonlinear, and Soft Matter Physics, 88(3):032107, 2013.